Evidence of a Hopf Bifurcation in Frog Hair Cells

M. Ospeck,* V. M. Eguíluz,† and M. O. Magnasco‡

*Biophysics Section, Laboratory of Cellular Biology, National Institute on Deafness and Other Communication Disorders, National Institutes of Health, Bethesda, Maryland 20892-0922 USA; †Center for Chaos and Turbulence Studies, The Niels Bohr Institute, DK2100 Copenhagen 0, Denmark; and ‡Laboratory of Mathematical Physics, The Rockefeller University, New York, New York 10021 USA

ABSTRACT The membrane potential of hair cells in the low-frequency hearing organ of the bullfrog, the amphibian papilla, sinusoidally oscillates at small amplitude in the absence of acoustical input. We stimulate the cell with a series of periodic currents close to this natural frequency and observe that its current-to-voltage transfer function is compressively nonlinear, having a large gain for small stimuli and a smaller gain for larger currents. Along with the spontaneous oscillation, this implies that the cell is poised close to a dynamical instability such as a Hopf bifurcation, because distant from the instability the transfer function becomes linear. The cell's frequency selectivity is enhanced for small stimuli. Simulations show that the cell's membrane capacitance is effectively reduced due to a current gain provided by this dynamical instability. We propose that the *Hopf resonance* is widely used by transducer cells on the sensory periphery to achieve small-signal amplification.

INTRODUCTION

In the frog's low-frequency hearing organ, the amphibian papilla, ~1000 hair cells in an epithelial sheet, mediate hearing in the frequency range of 50–1250 Hz in which the animal's call spectrum occurs (Rieke et al., 1995, 1997; Smotherman and Narins, 1999). We analyzed the rostral portion of the amphibian papilla, where 50–250 Hz electrically resonant hair cells reside. Electrically resonant hair cell behavior was first investigated in the turtle cochlea by Crawford and Fettiplace, in which they modeled the cell as a resonant tank circuit (Crawford and Fettiplace, 1980, 1981a, b). Looking at the large-signal regime they showed that the cells used a linear second-order electrical resonance, which endowed them with frequency selectivity.

A characterization of the ion channels which make a hair cell electrically resonant was obtained via studies of the bullfrog sacculus, a receptor for ground-borne vibration and low-frequency sound (Lewis and Hudspeth, 1983). A conductance-based model of an electrically resonant, saccular hair cell was then constructed (Hudspeth and Lewis, 1988a, b). Subsequently, the ion channels of the frog's low-frequency hearing organ, the amphibian papilla, were characterized and found to be very similar to those of the sacculus (Smotherman and Narins, 1999). However, both the turtle and bullfrog studies investigated the response to relatively large stimuli and implicitly considered the small-signal behavior as being linear.

Although the hair cell's electrical resonance and frequency selectivity are well understood, a problem remains. The nervous system can detect a hair cells' response only when the receptor potential is great enough to sufficiently activate Ca^{2+} channels to release neurotransmitter at the afferent synapse. To compensate for the cells' relatively large membrane capacitance an amplifier might be expected to enhance small responses. We describe how this amplifier is based upon poising the cell on a dynamical instability.

METHODS

Amphibian papillas were dissected from adult North American bullfrogs (*Rana catesbeiana*) in a standard saline solution containing 300 μM amiloride. By reversibly blocking the hair cells' transduction channels (Jorgensen and Ohmori, 1988) amiloride minimizes the cells' metabolic load during dissection. The tectorial membrane was removed after a 20-min digestion in 40 μg/ml protease (Sigma type VIII or type XXIV, Sigma-Aldrich Co., St. Louis, MO). The amphibian papilla was then allowed to rest in standard saline solution with amiloride for 10 min before being transferred to standard saline solution for experimental recording.

Hair cells were viewed at 800× magnification with differential-interference contrast optics on an upright microscope (MPS, Carl Zeiss, Inc., Oberkochen, Germany). To protect the preparation from photodamage, the illumination pathway was equipped with an infrared-reflecting hot mirror and a 10% transmitting neutral-density filter (Edmund Industrial Optics, Barrington, NJ). Conventional microelectrodes fabricated on a puller (Sutter P-80, Sutter Inst. Co., San Rafael, CA) displayed resistances of 300–500 MΩ when filled with 3 M potassium acetate solution. Electrode solution containing KCl was avoided because it degraded the cells' electrical oscillations. The tips of the microelectrodes were bent at ~60° to fit under the 40× water-immersion microscope objective lens with a numerical aperture of 0.75 (Hudspeth and Corey, 1978). Membrane currents were measured by two independent circuits in the amplifier Axoclamp 2-A (Axon Instruments, Inc., Burlingame, CA); the virtual-ground measurement closely agreed with the standard current monitor. The microelectrode's resistance was fully compensated and its capacitance 70% compensated.

Input and output waveforms were digitized at 5 kHz. The drive current command was filtered by two cascaded 8-pole Bessel low-pass filters set to a cutoff frequency of 1 kHz. A 10-fold voltage divider applied to the command current allowed for an ~3-bit description of a 2 pA current. The amplifier's current and membrane voltage outputs were amplified 10-fold and filtered before digitization by single 8-pole Bessel low-pass filters with a cutoff frequency of 1 kHz. The membrane-potential response was output to a spreadsheet program (Excel 97, version 8.0a, Microsoft Corporation, Redmond, WA) where 2048-point fast Fourier transforms (FFT) were

Received for publication 13 April 2000 and in final form 1 March 2001.

Address reprint requests to Dr. Mark Ospeck, NIDCD/NIH, Bldg. 9, Rm. 1E120, 9 Center Dr., MS C0922, Bethesda, MD 20892. Tel.: 301-496-7232; Fax: 301-480-0827; E-mail: ospeckm@nidcd.nih.gov.

0006-3495/01/06/2597/11 $2.00

performed during the experiment to measure the frequency of the free-running voltage oscillation.

Heights of frequency-resolved peaks from the FFT were voltage-calibrated and then used to plot *V-I* transfer functions when stimulating the cell with an external current. At a sampling rate of 5 kHz our 2048-point FFT had a frequency resolution of 2.4 Hz. We calibrated peak heights for frequency-resolved peaks (3 Hz full-width at half-maximum (FWHM) power) by first outputting sine waves directly from the A to D to the D to A. However, in our experiments the voltage oscillations in hair cells would refuse to phase-lock to currents at or below 2 pA, instead persisting with their own spontaneous voltage oscillation (fluctuating 3–7 Hz FWHM power width). Phase-locking to our stimulus current was signaled both by a sharpening of the FFT peak to the 3 Hz limit and a sharp increase in gain. Above 2 pA of stimulus current our experimental FFT peaks sharpened to this 3 Hz FWHM power width and we checked that they accurately represented the peak-to-peak size of a voltage oscillation phase-locked to our current stimulus.

Current stimuli were provided and responses were recorded by a computer (P6400 GX1, Dell Computer, Round Rock, TX) running LabVIEW software (version 5.0, National Instruments, Austin, TX). Because large voltage responses are asymmetrical, the magnitudes of current stimuli and voltage responses are reported as peak-to-peak values except when otherwise noted as being amplitudes. Simulations were performed using Mathematica (version 4.0, Wolfram Research, Inc., Champaign, IL).

RESULTS

Experimental *V-I* curves

When impaled with conventional microelectrodes, hair cells of the rostral portion of the bullfrog's amphibian papilla typically had resting potentials near −55 mV. Even in the absence of stimulation, most such cells displayed membrane-potential oscillations. We recorded electrical oscillations from ~150 hair cells, many of which were also stimulated by injection of a sinusoidal current several picoamps (pA) in magnitude and close to the cells' frequency of spontaneous oscillation. We then performed an FFT on the membrane potential and plotted the voltage response against the stimulus current to produce a cell's dynamic voltage-current relation (see Methods).

Hair cells can be viewed as current-to-voltage converters, and gain in this context corresponds to input impedance. Here we distinguish signal gain, the cell's input impedance Z_{in}, as the slope of the chord between a point on the *V-I* transfer function and the origin, versus slope gain, the local slope of the *V-I* transfer function.

One would expect that a freely oscillating resonator would provide a large gain to a small input signal at its natural frequency. A hair cell spontaneously oscillating at 126 Hz (Fig. 1 *A*) provides a large slope gain to a small 126 Hz stimulus current (Fig. 1 *B*). We twice stimulated the cell with series of currents at its resonance frequency. At resonance in the vicinity of a 4 pA stimulus current the cell has a slope gain of 1 GΩ and a Z_{in} of 0.5 GΩ. Hair cells in the rostral amphibian papilla are large, ~30−40 μm in length, and as such have a typical capacitance of 15 pF (Smotherman and Narins, 1999), resulting in a capacitive input impedance of only 80 MΩ for a 126 Hz input current ($Z_{in} = 1/(j\omega C)$). However, because the observed input impedance, 0.5 GΩ, exceeds that of the capacitive contribution, it appears that this cell amplifies 4 pA input currents by a factor of 6, thereby effectively shrinking its own capacitance.

An oscillation with a high quality factor (Q) requires many cycles to build up and many to decay. Small-signal gain is accomplished by the cell appearing as a high-Q resonant filter in which the voltage response from each cycle of stimulus current is added to the previous cycle's response to build up a large total response (Fig. 1 *D*). Q is significantly reduced for a 21 pA stimulus, which is consistent with this input receiving less gain (Fig. 1 *E*).

Although one might expect qualitatively similar response functions close to the resonance, we wish to distinguish an on-resonance from a near-resonance transfer function. Shown are *V-I* curves for three series of stimuli where the topmost series is driven on resonance with a slope gain of 1.1 GΩ in the vicinity of 8 pA (Fig. 2 *B*). The middle series is stimulated only 7 Hz above the resonance and shows a characteristic sawtooth structure that mixes high-gain sections (slope gain >1 GΩ) with sections where the stimulus appears to be unable to engage the nonlinear resonance. The sawtooth-shaped *V-I* curves were repeatable and occurred on >10 occasions when the resonance frequency was missed by 5–10 Hz.

In addition to a nonlinear *V-I* transfer function exhibiting large-signal dynamic range compression, a possibly related change occurs as the stimulus amplitude increases: large currents typically induce tonic hyperpolarizing shifts in membrane potential. The two resonance series shown in Fig. 2 *B* had a −1.2 ± 0.1 mV d.c. shift for a 48-pA drive current, and a −2.0 ± 0.1 mV d.c. shift for a 96-pA stimulus. A second hair cell's two resonance series had a −1.5 ± 0.1 mV d.c. shift for a 58-pA stimulus, and a −3.8 ± 0.6 mV d.c. shift for a 116-pA stimulus. Below a 30-pA stimulus current any d.c. shift was concealed by voltage noise. The shift is important because the natural frequency of the electrically resonant hair cell has been shown to be a strongly increasing function of average membrane potential (20 Hz/mV; Hudspeth and Lewis, 1988a).

Current stimuli at or below 2 pA are unable to entrain the cell's voltage oscillation and show little gain. Data points from the transfer functions (Figs. 1 *B* and 2 *B*) are the FFT amplitude from the average of five data sets and thus represent the membrane potential response to several hundred cycles of stimulus current. Data points from 2-pA stimuli without this averaging show both the voltage response locked to the stimulus frequency and the unlocked free oscillation at the natural frequency. In these experiments (not shown) the 2-pA stimuli do not entrain or interfere with the free oscillation, but simply beat against it. At ~3 pA entrainment begins and a large slope gain results.

The hair cell's ability to actively gain small current stimuli requires input power. Both amiloride, a known transduction channel blocker, or an ~50-pA hyperpolariz-

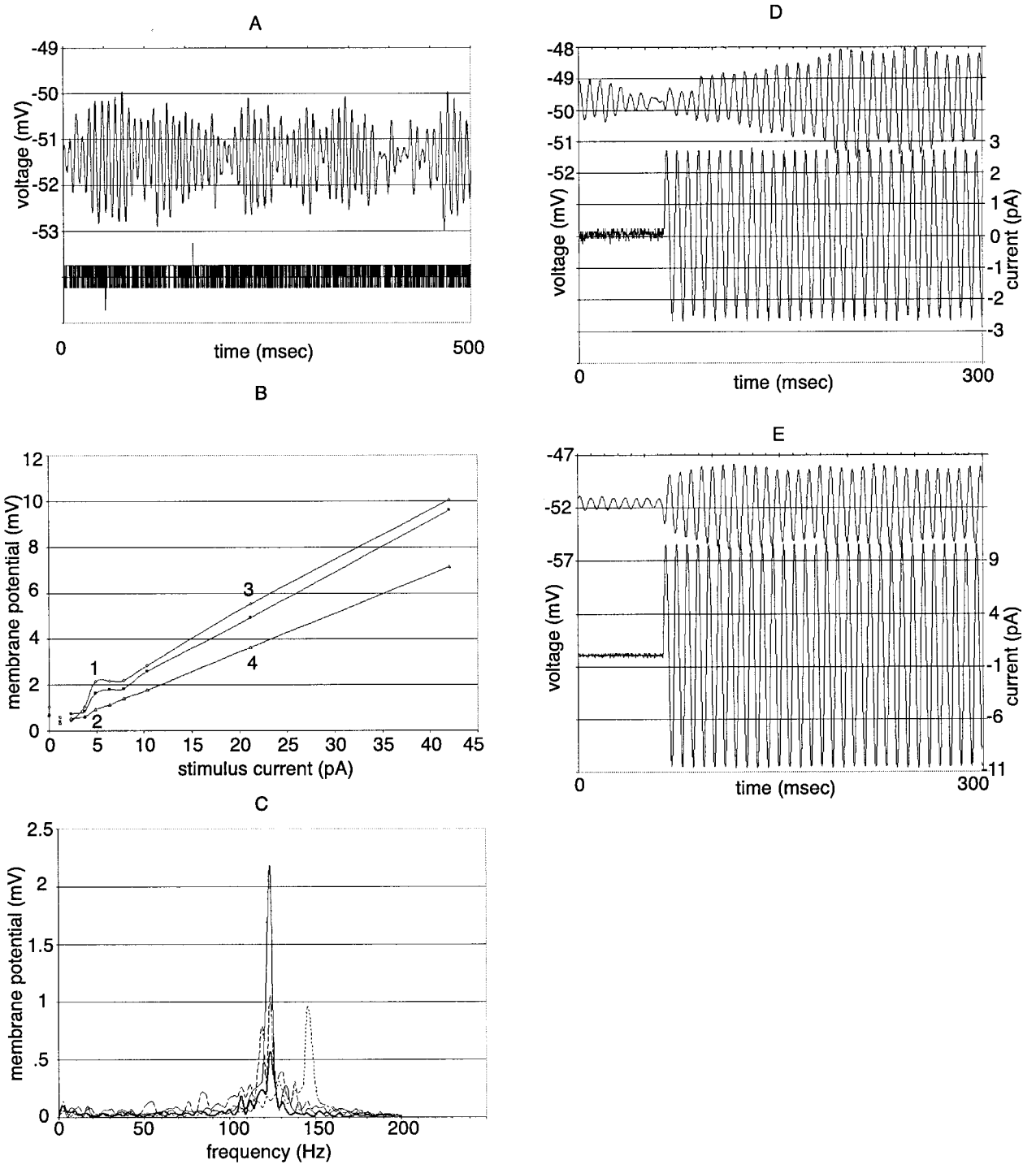

FIGURE 1 Experiment showing spontaneous membrane potential oscillations and large small-signal gain. (*A*) A hair cell oscillating without input at 126 Hz. Shown below is the stimulus current, which is zero, but has 0.5 pA of digitization noise. The cell rested at ~ -51 mV. (*B*) *V-I* transfer functions for the cell stimulated once with a series 20 Hz above resonance (*bottom ramp*) then twice with a series of currents at its resonance frequency (top recorded 5 min later, then middle 5 min after top). At resonance the cell has a large small-signal slope gain of 1 GΩ in the vicinity of a 4-pA stimulus. Each driven data point is the FFT amplitude of the average of five 410-ms-long data sets, and so represents the average membrane potential response to 250 cycles of stimulus current (see Methods). (*C*) Four 2048 point FFTs: *long-dashed line*, before resonance stimulus series; *solid line*, high-*Q* response (point 1 in *B*); *thick solid line*, after resonance stimulus series; *short-dashed line*, response when stimulated 20 Hz above the resonance frequency (point 2 in *B*). (*D*) For small input the cell acts as a high-*Q* resonant filter in which the voltage response from each cycle of stimulus current is added to the previous cycles' to build up a large total response (point 1 in *B*). (*E*) Onset *Q* becomes smaller when the stimulus is larger (point 3 in *B*).

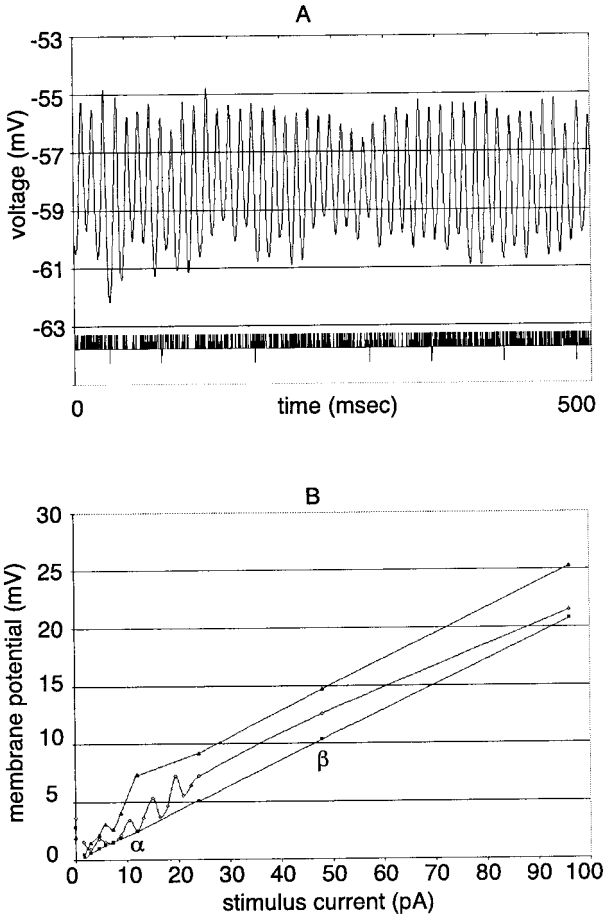

FIGURE 2 Experiment distinguishing on-resonance from near-resonance *V-I* transfer functions. (*A*) A hair cell with a large 88-Hz spontaneous voltage oscillation. Stimulus current shown below is zero, but has 0.5 pA of digitization noise. (*B*) *V-I* curves for three experiments. Each data point is the FFT amplitude of the average of five 410-ms-long data sets and thus represents the membrane potential response to 190 cycles of stimulus current (see Methods). The topmost series was driven on resonance and showed a small-signal slope gain of 1.1 GΩ. The middle series was driven 7 Hz above resonance and showed a characteristic sawtooth structure that mixed high slope gain sections (>1 GΩ) with sections where the stimulus appeared unable to engage the nonlinear resonance. The bottom series was driven 45 Hz above resonance and behaved like an ohmic 200-MΩ ramp. The order of recording was top, middle, bottom, taking in all 20 min.

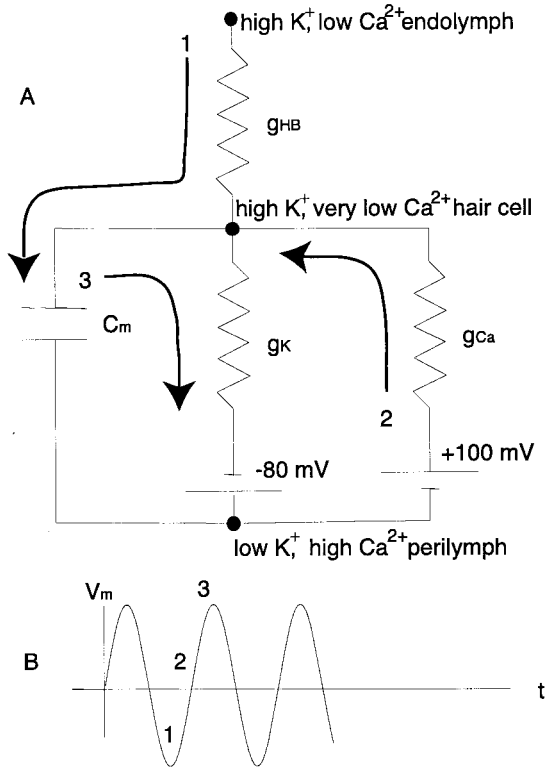

FIGURE 3 (*A*) Circuit diagram of the membrane oscillator model of an electrically resonant hair cell. g_{HB} is the quiescent hair bundle conductance passing a cation current that charges cell capacitance C_m. gC_a is a fast voltage-gated Ca^{2+} conductance whose reversal potential accounts for a 100-mV battery driving Ca^{2+} into the cell. g_K represents Ca^{2+}-gated K^+ conductance whose reversal potential, a −80-mV potassium battery, drives K^+ out of the cell. (*B*) Spontaneous membrane potential oscillation occurs when the quiescent hair bundle conductance g_{HB} is made large enough. Large g_{HB} causes a small negative voltage perturbation undershooting the "resting" potential to grow into a free oscillation because then the voltage-driven bundle current is sufficiently large to cause an even larger overshoot when the membrane potential rebounds. Consider a spontaneous oscillation in progress: when the cell hyperpolarizes, the K^+ channels are turned off due to lack of Ca^{2+} and the voltage-driven K^+ current through the transduction channels begins to charge the cell capacitance (1). This depolarization turns on a voltage-dependent Ca^{2+} current, which further acts to depolarize the cell (2). The Ca^{2+}, however, turns on Ca^{2+}-gated K^+ channels with a time delay and their large outward K^+ current then hyperpolarizes the cell (3), restarting the cycle.

ing d.c. current will eliminate both the hair cell's spontaneous voltage oscillations and its large small-signal gain, indicating that excitability is a strong function of the positive current into the cell (experiments not shown).

Membrane oscillator model; canonical Hopf bifurcation model

A seven-dimensional conductance-based model has been proposed to explain electrically resonant hair cell behavior (Fig. 3; Appendix; Hudspeth and Lewis, 1988a, b). This membrane oscillator model uses three conductances: mechanically gated, cation-specific transduction channels that are in contact with K^+-rich endolymph, tensioned 30% open at rest, and inputting a positive current into the cell; voltage-dependent Ca^{2+} channels in contact with Ca^{2+}-rich perilymph; and large-conductance K^+ channels also in contact with low-K^+ perilymph and gated open by internal Ca^{2+}. Here, we write only the membrane oscillator's capacitor-charging equation:

$$-C_m V'_m[t] = g_{Ca}\, m[t]^3\, (V_m[t] - e_{Ca}) + g_K\, (p_{K4}[t] + p_{K5}[t])\, (V_m[t] - e_K) + (g_{HB} + dg_{HB} \sin[2\pi f t]) V_m[t] \quad (1)$$

g_{Ca}, g_K, and g_{HB} charge/discharge the hair cell's membrane capacitance C_m. The calcium channel conductance, g_{Ca}, has an open probability controlled by the voltage-dependent subunit conformation probability m[t] and a reversal potential e_{Ca}, which is typically +100 mV. The large-conductance Ca^{2+}-gated K^+ channel g_K is represented by a five-state linear model in which the occupancy of states 4 and 5 gives the total open probability, and the channel's reversal potential e_K is −80 mV. The conductance of the quiescent transduction channels g_{HB} has a reversal potential of ~0 mV (Corey and Hudspeth, 1979). A periodic hair bundle conductance oscillation is represented as $dg_{HB} \sin[2\pi f t]$.

The model's parameter values had originally been set to account for the low-*Q*, second-order electrical resonance observed in hair cells of the bullfrog sacculus that do not oscillate at rest. However, experiments on hair cells of the amphibian papilla show spontaneous sinusoidal membrane potential oscillations and a compressively nonlinear *V-I* transfer function with a large voltage gain for a small stimulating current—this gain being due to the cell's having a high *Q* voltage response only for small currents at the natural frequency. Taken together, these three indicate that the cells are operating near to a dynamical instability called a Hopf bifurcation.

A supercritical Hopf bifurcation occurs when $\mu = 0$ for the canonical two-dimensional *r*, θ system (Fig. 4; Strogatz, 1994):

$$\dot{r} = \mu r - r^3 \qquad \dot{\theta} = \omega_0 + br^2 \tag{2}$$

This minimal dynamical system has three parameters with ω_0 setting the natural frequency, and *b* accounting for a decrease in natural frequency with increasing oscillation amplitude. The control parameter μ sets excitability. When $\mu < 0$ the system relaxes to the origin, an attracting fixed point. The closer μ is to 0, the slower and higher *Q* is this relaxation. For $\mu > 0$ the origin becomes a repelling fixed point, and an oscillatory attractor of size $r_{l\text{-}c} = \mu^{1/2}$ is created (called a limit-cycle). Again, the closer μ is to 0 the slower will be the relaxation to this limit-cycle. At the bifurcation where $\mu = 0$ a small impulsive kick to the system will oscillate forever, having an infinite *Q* ($= \omega_0/(2\mu)$). It is clearly advantageous for an amplifier to operate in the vicinity of the bifurcation because there a weak periodic forcing will be built up into a large response due to the superposition of the high-*Q* oscillations from each stimulus cycle. Periodically forcing this system at the bifurcation and at its natural frequency results in a transfer function having a cube root dependence on stimulus amplitude, while forcing when only close to the bifurcation nets a faint-signal, high-gain linear regime joined onto a compressive nonlinearity for larger input (Eguíluz et al., 2000). There are three characteristics of the response when forcing the canonical Hopf model: both slope gain and resonance frequency decrease and the resonance width increases as stimulus amplitude is increased.

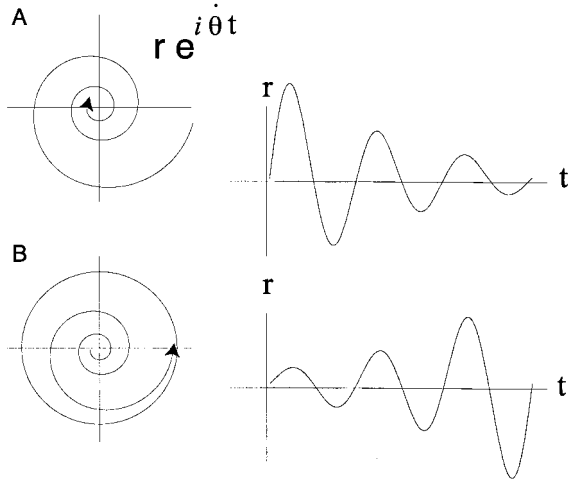

FIGURE 4 Canonical supercritical Hopf bifurcation for the two-dimensional *r*, θ system: $\dot{r} = \mu r - r^3$, $\dot{\theta} = \omega_0 + br^2$. (*A*) The dynamical system spirals in toward a fixed point attractor when the control parameter μ is less than zero. (*B*) The system spirals away from the now-repelling fixed point and toward a stable limit-cycle attractor when μ is greater than zero. A supercritical Hopf bifurcation occurs when $\mu = 0$, and this is also where the system is most unstable to perturbation, and therefore the most sensitive.

In the Appendix we show that the membrane oscillator can be poised at a supercritical Hopf bifurcation. We linearize the oscillator about a relevant fixed point and find out which of its eigenvalues has the least negative real part, which turns out to be the complex pair λ and λ^*. A Hopf bifurcation occurs by definition when such a pair crosses the real axis (Strogatz, 1994); $\exp[\lambda t]$ gives the time dependence of the dynamical system in the vicinity of the fixed point where the control parameter ($\mu = \mathrm{re}[\lambda]$) and angular frequency ($\omega_0 = \mathrm{im}[\lambda]$) are functions of the system parameters. Near the oscillator's fixed point its dynamics are exactly like those in the vicinity of the canonical Hopf bifurcation.

Oscillator natural frequency depends essentially on the rate constants of the Ca^{2+}-gated K^+ channel, which is consistent with experiment (Rosenblatt, et. al., 1997). The parameter clock (*clk*) multiplied all of these rate constants and was used to adjust the natural frequency. For most simulations we chose a 109 Hz oscillator (*clk* = 0.6) because the rostral amphibian papilla is sensitive to the fundamental tone of the bullfrog's call spectrum, which is ~100 Hz (Rieke et. al., 1997).

We made two parameter changes in the saccular hair cell membrane oscillator model that increased oscillator excitability to account for amphibian papilla hair cell behavior. Most importantly, we limited leak conductance to bundle conductance, causing its reversal potential to be shifted positive by 30 mV. Additionally bundle conductance was increased from 1 to 1.4 nS, placing the oscillator very close to a Hopf bifurcation at 109 Hz (*clk* = 0.6, g_{HB} = 1.4 nS). When increasing natural frequency it was found necessary

to increase bundle conductance to maintain excitability. There are many other system parameter variations that will increase excitability (control parameter μ near 0), such as increasing the Ca^{2+} conductance or increasing Ca^{2+} channel voltage sensitivity. A 30-mV positive shift in leak conductance reversal potential was chosen because hair cells in the rostral amphibian papilla, unlike saccular hair cells, lack I_{K1} inward rectifiers (Smotherman and Narins, 1999), which would act as a K^+ leak conductance and hyperpolarize the cell to ~ -70 mV (Holt and Eatock, 1995).

Performance of the oscillator near a Hopf bifurcation; comparison to experiment

The phase relationship between the stimulus current and the membrane potential response depends on the frequency difference between the stimulus and the natural frequency. There is a well-understood region in stimulus frequency, amplitude space called an Arnold tongue, where a stimulus is able to entrain the resonance (Glass and Mackey, 1988). This 1:1 lock-in tongue is a triangular region centered at the natural frequency and growing wider while bending toward lower frequency with increasing stimuli. A small natural frequency stimulus current will sit in the middle of the tongue and will lead the membrane potential by 90° because the hair cell is a capacitive load. A stimulus frequency higher than the natural frequency will lead by $>$90°, while a lower frequency stimulus will lead by $<$90°. Stimuli outside of the tongue will be unable to capture the resonance and so a beat will be generated between the natural frequency and the stimulus frequency.

A high-*Q* resonator requires that a portion of the response from the previous stimulus cycle is added to the response to the next so that a large total response can be built up. A natural frequency stimulus current leading the membrane potential by 90° when locked is shown along with its response, a high-*Q* potential oscillation (Fig. 5 *B*; compare also to the experiment shown in Fig. 1 *D*, which locks with a 100° phase lead). At a potential peak the voltage-dependent Ca^{2+} conductance is increased so that with a 90° phase delay the Ca^{2+}-gated K^+ conductance will increase and thus the potential will fall further for the next current downstroke. This hysteresis, whereby a conductance memory of the previous half-cycle is passed to the next, forms the basis for the oscillator's obtaining a small-signal, high-*Q* response.

Dynamically, a Hopf bifurcation means that a fixed point becomes unstable with a complex pair of eigenvalues, i.e., oscillates. Proximity to the bifurcation means that the time to reach the periodic solution after a perturbation is much larger than the period of the oscillation, being theoretically infinite at the bifurcation. In our experiment (Fig. 1 *D*) the hair cell takes 17 stimulus cycles to reach the periodic solution, while in the simulation (Fig. 5 *B*) the cell takes 8 cycles—thus in both cases the oscillator is poised close to a bifurcation.

The oscillator's large small-signal gain when it is poised on a Hopf bifurcation and stimulated at its natural frequency originates from a strong coupling between membrane potential and membrane resistance (Fig. 5 *C*). In this parametric plot the quiescent system is a very high *Q* fixed point. The smallest ring surrounding this fixed point is the oscillator's response to a 2.1-pA natural frequency stimulus current. In this case one additional picoamp enters the cell leading the potential peak by 90° and the net result is a -4% change in the whole cell K^+ conductance, thereby blocking 19 pA from leaving. Thus the one additional picoamp of bundle current has been amplified 20×. Although we would expect the cell's 15-pF capacitive load at 109 Hz to give it an input impedance of 100 MΩ, the cell actually obtains a 2.3-mV amplitude response for only a 1.0-pA amplitude current ($Z_{in} = 2.3$ GΩ). Notice that it is in fact necessary for the cell to run a large 79-pA quiescent current so that it is then able to turn off a large fraction of this current and thereby obtain a current gain.

The low-gain, large-signal regime is due to a simple current multiplier in which hair bundle current engenders a fast Ca^{2+} current. In this large-signal regime the dimensionless ratio of the change in K^+ conductance resulting from a change in bundle conductance is small ($dg_K/dg_{HB} = -0.27$, Fig. 5 *C*, second-largest ring), while in the small-signal regime this ratio is large ($dg_K/dg_{HB} = -17$, Fig. 5 *C*, smallest ring).

At parameter values where spontaneous oscillations begin to show, the oscillator has the cube-root shaped transfer function expected of a dynamical system poised at a Hopf bifurcation (Fig. 5 *D*; Eguíluz et al., 2000). Experimentally, however, the hair cell is usually seen below the bifurcation, having a typical small-signal slope gain = 1 GΩ and large-signal slope gain = 250 MΩ. If we force an oscillator poised slightly below the bifurcation at 2 Hz above its natural frequency, then we can match the asymptotic slope gains and the location of the cross-over region of the Fig. 1 *B* experiment (crosses, Fig. 5 *D*).

Consistent with the canonical Hopf resonance, the oscillator has a very sharp small-signal frequency selectivity at

FIGURE 5 Simulations of a 109-Hz membrane oscillator (*clk* = 0.6), which can be poised at a Hopf bifurcation ($g_{HB} = 1.4$ nS). (*A*) A bifurcation diagram showing Hopf bifurcations occurring at both 1.4- and 2.3-nS hair bundle conductance. (*B*) At the bifurcation an 8.4-pA stimulus results in a high-*Q* voltage oscillation, which takes about eight stimulus cycles to reach its peak size. At each potential peak the voltage-dependent Ca^{2+} conductance increases so that with a delay the Ca^{2+}-gated K^+ conductance will increase and the potential will fall farther for the next current downstroke. Gain is accomplished by a conductance memory of the previous half-cycle being passed on to the next. (*C*) Large small-signal gain results from a strong coupling between membrane potential and membrane resistance. Shown is a parametric plot of membrane potential versus Ca^{2+}-gated K^+ channel open probability. The

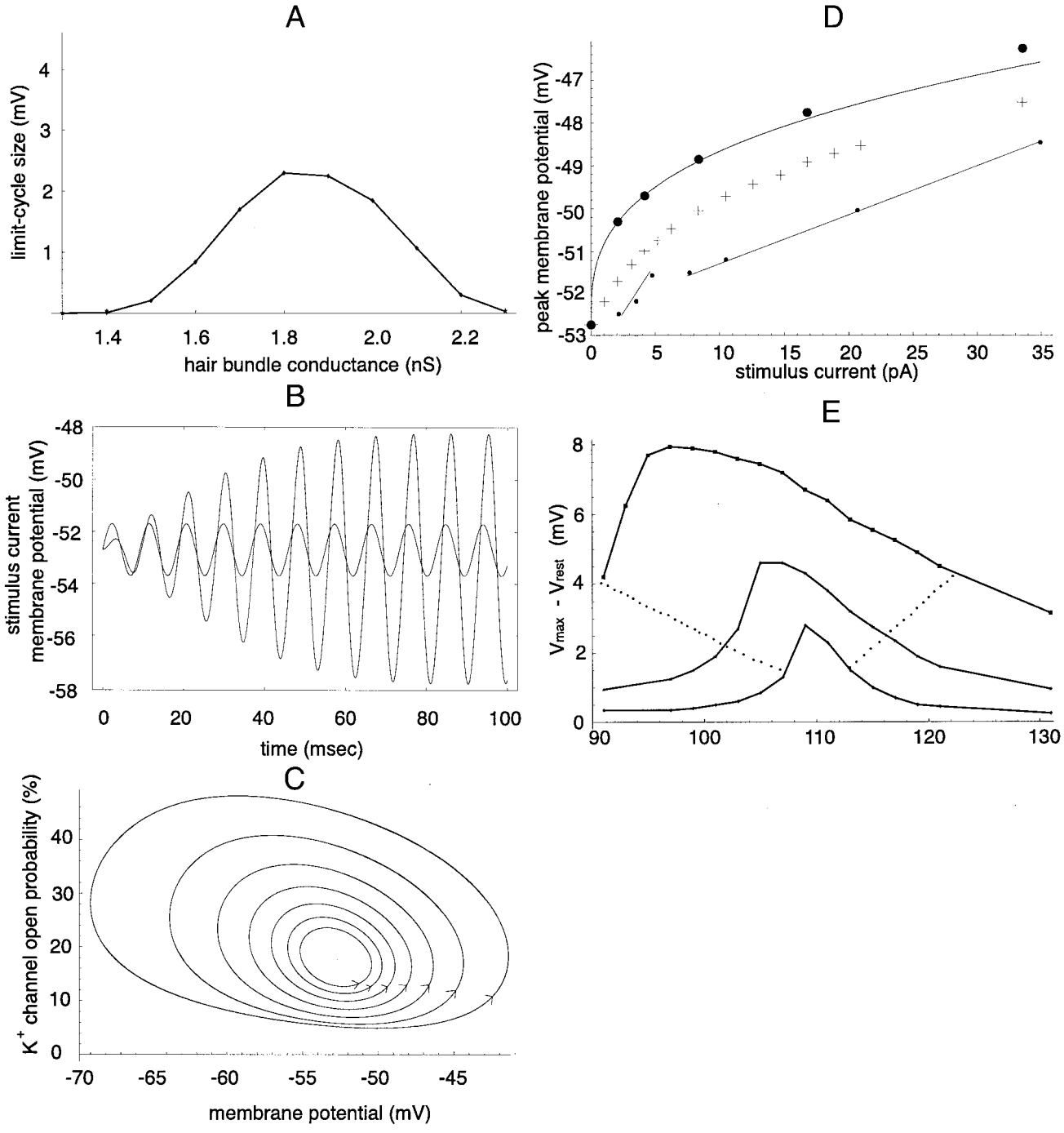

oscillator is poised as a high-*Q* fixed point resting at −52.7 mV and 17% K^+ channel open probability. Each ring surrounding the operating point results from doubling the size of the previous natural frequency conductance oscillation. The smallest ring is the response to a 20-pS amplitude conductance oscillation. $dg_{HB}\ V_m$ = (20 pS)(−52.7 mV) = −1 pA, which results in K^+ channel open probability dropping from 17 to 13%. $(-4\%)g_K$ (−52.7 mV $-e_K$) = (−4%) 17 nS (−52.7 mV − −80 mV) = −19 pA. Hence, bundle current is amplified 20×. (*D*) *V-I* transfer function (*large points*) for a 109 Hz oscillator when poised where it begins to show spontaneous oscillations and is driven at its natural frequency. It is well-fit by a cube root (*curve*), the expected shape when forcing at a Hopf bifurcation. However, experimentally the cell is only close to the bifurcation, having a typical small-signal slope gain = 1 GΩ and large-signal slope gain = 250 MΩ. If instead we force 2 Hz above its natural frequency, a 128-Hz oscillator poised slightly below the bifurcation, we obtain the same asymptotic slope gains and cross-over region location as the Fig. 1 *B* experiment (crosses; *clk* = 0.85, g_{HB} = 1.4 nS). Compare this to a replot of the top data set from the Fig. 1 *B* experiment (*small points*), noting that gain obtains only with phase-locking and that noise prevents experimental phase locking at or below 2 pA, which results in the 0.8-mV offset discrepancy between experiment and simulation. (*E*) Sharp small-signal frequency selectivity of the oscillator at the bifurcation (2.1-pA stimulus, *bottom curve*). As the stimulus is increased, first to 8.4 and then to 33.6 pA, both the resonance frequency and the gain decrease, and the width of the resonance increases. The dotted lines between the half-maximums of the resonance curves describe an inverted triangular region similar to an Arnold lock-in tongue.

the bifurcation (Fig. 5 *E*, 2.1 pA stimulus). As the stimulus is increased the width of the resonance dramatically increases, which is consistent with experiment: compare data points 2 and 4 in the Fig. 1 *B* experiment and also points α and β in the Fig. 2 *B* experiment. Both points 2 and α lie outside of the resonance half-maximum response, while 4 and β both lie within the resonance half-maximum.

The natural frequency of the canonical Hopf resonance drops with increased forcing, and we observe the oscillator's resonance peak dropping in frequency due to large stimuli causing hyperpolarizing d.c. shifts, which slow down the voltage-dependent rate constants on the Ca^{2+}-gated K^+ channels (Fig. 5 *E*). A large positive voltage will flood the cell with Ca^{2+} so as to turn on its Ca^{2+}-gated K^+ channels sufficiently to cause an even larger negative voltage excursion. Large voltage oscillations are asymmetrical in a $+2$ to -3 ratio both in experiments and in simulations (Fig. 5 *C*).

An interesting phase shift occurs at the bifurcation for very small stimuli exactly on resonance. A 2.1-pA stimulus will be exactly in phase with its potential response, which means that the cell has become a resistive load. The current gain for this small resonant frequency input is very large ($\sim$23) so that the effective cell capacitance has been very much diminished. In this simulation the hair cell has a transition from being a capacitive load at an 8.4-pA stimulus to a resistive load for 2.1 pA. However, likely due to noise, 2-pA experimental stimuli were unable to entrain, or phase-lock, to the nonlinear resonance.

Simulations including both current and voltage noise could qualitatively reproduce the experimentally observed spontaneous voltage oscillations. We performed simulations in the presence of 100-μV RMS voltage noise and $\pm$1% g_{HB} noise across a 500-Hz bandwidth. The experimental trace shown in Fig. 1 *A* behaved the same as a high-*Q* fixed point driven by noise, called a Hopf precursor ($\mu < 0$; Fig. 6 *A*; Neiman et al., 1997). The large oscillatory behavior of the Fig. 2 *A* experiment was reproduced by a limit-cycle being buffeted by noise ($\mu > 0$; Fig. 6 *B*).

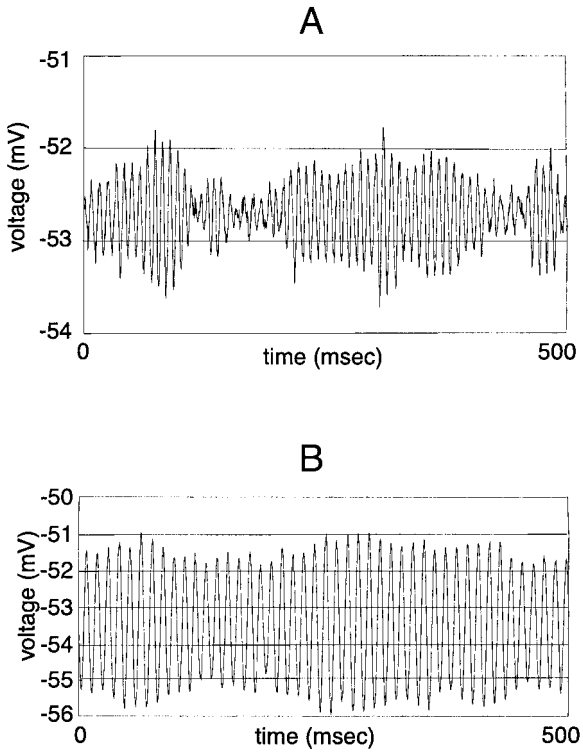

FIGURE 6 The oscillator in the presence of 100 μV RMS voltage noise and $\pm$1% hair bundle conductance noise across a 500-Hz bandwidth. (*A*) The oscillator was poised as a 128-Hz fixed point slightly below the bifurcation and then subjected to noise (clk = 0.85, g_{HB} = 1.4 nS; same parameter set as Fig. 5 *D* crosses). Only by poising the oscillator below the bifurcation could we qualitatively reproduce the Fig. 1 *A* experimental trace. (*B*) The oscillator was poised above the bifurcation as a 3.5-mV, 88-Hz limit-cycle and then buffeted by noise (clk = 0.35, g_{HB} = 1.4 nS. g_{Ca} = 5.0 nS; compare to Fig. 2 *A* experiment).

DISCUSSION

K^+ channel voltage-conductance instability

Capacitance can be thought of as a voltage inertia that acts to damp voltage fluctuations. The Ca^{2+}-gated K^+ channel acts like a capacitance in that a depolarizing voltage fluctuation causes a delayed increase its open probability, resulting in hyperpolarization and apparent negative feedback. However, for a single frequency this delayed hyperpolarization constitutes positive feedback, being properly timed to assist in the waveform's next downstroke. Consider a hyperpolarizing voltage fluctuation: if the quiescent hair bundle sources enough positive current and the K^+ channel is sufficiently voltage-sensitive (via Ca^{2+}), then it will turn off enough that the bundle current will then generate a positive rebound response larger than the original hyperpolarizing fluctuation. This overshooting response of the K^+ channel is responsible for a voltage fluctuation growing to a limit-cycle above the bifurcation and the high-*Q* small-signal gain of the oscillator in the vicinity of the bifurcation.

Shape of the transfer function near the bifurcation

In our experiments the hair cell is not located at the bifurcation, but rather behaves as a noisy high-*Q* fixed point or a small noisy limit-cycle (Figs. 1 *A* and 2 *A*). Likely due to noise, a 2-pA natural frequency stimulus appears unable to entrain the nonlinear resonance (Figs. 1 *B* and 2 *B*). When the stimulus is larger a narrow range of stimuli will then be able to engage the nonlinear resonance and obtain a large small-signal gain. However, because the system is not exactly at the bifurcation, these data points will lie along a high-gain, linear transfer function (crosses, Fig. 5 *D*; Eguíluz et al., 2000). Gain compression appears as the stimulus continues to increase ($\sim$7 pA in the Fig. 1 *B* experiment and

~15 pA in the Fig. 2 *B* experiment). Still larger stimuli cause the natural resonance peak to drop in frequency, effecting a loss of the nonlinear resonance and a return to the second-order resonance linear *V-I*.

On more than 10 occasions sawtooth-shaped *V-I* transfer functions were observed that were repeatable and always associated with 5–10-Hz misses of the natural frequency (Fig. 2 *B*, *middle series*). They appear as an alternation of high slope gain sections (>1 GΩ) from engagement of the nonlinear resonance with low gain pieces (~200 MΩ) from engagement of the linear second-order resonance. In simulations the 1:1 lock-in tongue is a smooth-edged triangle, opening at 1 Hz/pA (Fig. 5 *E*). We note that the 1:1 experimental tongue has a complicated boundary and speculate that its edge does not grow in a monotonic fashion with stimulus.

Feedback to poise the membrane oscillator near to the bifurcation

One minimal scheme for dynamically poising the amplifier close to the Hopf bifurcation is via the integration of a Ca^{2+} error signal. Consider the system oscillating with a several-millivolt limit-cycle. As Ca^{2+} begins to saturate the cell's buffering capacity it slowly accumulates, so that after a number of cycles the Ca^{2+}-gated K^+ channel is shifted toward oscillating about a larger open probability. This in turn causes a hyperpolarizing d. c. shift in membrane potential, which reduces both the Ca^{2+} channel operating point's open probability and the size of its oscillation about that point. A smaller limit-cycle results until finally the buffer has had time to sweep up all of the excess Ca^{2+}, thereby shifting K^+ channel open probability downward. Now membrane potential increases, increasing the size of the Ca^{2+} channel oscillation, which then increases the size of the K^+ channel oscillation, finally causing the voltage oscillation to return to a medium-sized limit-cycle, until once again the Ca^{2+} buffer is overloaded. Schemes similar to this one have been proposed in regard to mechanical hair bundle limit-cycle oscillations (Martin and Hudspeth, 1999) and have been referred to as "self-tuned critical oscillations" (Camalet et al., 2000). If we reintroduce the control parameter μ as a slow dynamical variable into the 2D canonical Hopf system, $d\mu/dt = -\mu[t]/\tau\, r[t]^2$, then we can generate a feedback attraction where the system seeks the bifurcation as its operating point.

Standard saline versus endolymph

In vivo, the hair cell's apical surface is bathed in a high K^+, low Na^+, low Ca^{2+} endolymph. We used a high Na^+, high Ca^{2+}, low K^+ standard saline vice endolymph bathing the apical surface as it proved too difficult to use a two-compartment recording chamber on the amphibian papilla. As a consequence we would expect the open probability of the transduction channels to drop from 30% to 15% due to the stereociliary adaptation motors seeing the high Ca^{2+} in the standard saline (Eatock et al., 1987). This should act to decrease excitability, which both experiments and simulations show to be a strong function of the quiescent positive current into the cell. Nevertheless, experiments show that the cell is able to maintain itself in the vicinity of a Hopf bifurcation, having spontaneous oscillations similar to those seen in previous experiments with endolymph bathing the hair bundle (Crawford and Fettiplace, 1980). One possibility is that the cell is able to adjust its Ca^{2+} buffer concentration because chicken hair cell cytoplasm is known to contain a high concentration of the Ca^{2+} buffer parvalbumin's messenger RNA (S. Heller, Rockefeller University).

The chief problem with standard saline appears to be that it places a high metabolic load on the cell so that the lifetime of a preparation where one can obtain a high-gain recording is ~1 h. The main problem with extensively mapping the shape of the nonlinear resonance is this lack of time, because long before the cell dies the resonance will begin to wander in frequency.

CONCLUSION

Electrically resonant hair cells of the bullfrog amphibian papilla are poised close to a Hopf bifurcation to obtain a compressively nonlinear transfer function having a large small-signal gain and a sharp small-signal frequency selectivity. Cochlear inner hair cells of a 20-day-old mouse contain a large, fast potassium conductance (Kros et al., 1998) with a strongly nonlinear *I-V* reminiscent of the large conductance potassium channel of the frog hair cell (Corey and Hudspeth, 1979), and it is this *I-V* nonlinearity that is the essential ingredient for a Hopf resonance in the amphibian papilla. Amphibian papilla hair cells electrically oscillate without bundle stimulation, and amplifiers that oscillate without input are typically used to provide a reference signal for a lock-in amplifier that is sensitive to faint signals only within a narrow range around its reference frequency (Gardner, 1979). Electroreceptors used by electric fish are derived from electrically resonant hair cells that have lost their mechanosensitivity (Meyer and Zakon, 1982) and paddlefish electroreceptors behave like noisy phase-locked loops (Neiman et al., 1999). The photoreceptor of the crawfish, when stimulated by light at its best frequency of 0.1 Hz, responds with trains of impulses, and this transfer function exhibits a compressive nonlinearity at very low levels of light input (Herman and Stark, 1963; Milhorn, 1966). The FitzHugh-Nagumo model of a nerve membrane includes a Hopf bifurcation (FitzHugh, 1962) and they appear to occur frequently. As these examples indicate, the Hopf resonance is probably widely used by sensory transducer cells due to its obvious advantages.

APPENDIX

Parameter values that will place the membrane oscillator model (Hudspeth and Lewis, 1988a, b) at a Hopf bifurcation, resulting in an extremely high Q fixed point at 109 Hz:

clk 0.6	g_{HB} 1.4×10^{-9} S	g_{Ca} 4×10^{-9} S
g_K 17×10^{-9} S	dg_{HB} 0×10^{-9} S	*f* 109 Hz
e_{HB} 0×10^{-3} V	e_{Ca} 100×10^{-3} V	e_K -80×10^{-3} V
C_m 15×10^{-12} F	*U* 0.02	*xi* 3.4×10^{-5}
K_s 2800 s^{-1}	*VT* 25.4×10^{-3} V	*vol* 1.25×10^{-12} L
Faraday 96485 Coul/mol	K_{Caa} 510 s^{-1}	K_{Cab} 940 s^{-1}
V_{Ca0} 70×10^{-3} V	V_{Caa} 8×10^{-3} V	V_{Cab} 6.2×10^{-3} V
$k_{Ca21init}$ 23000 s^{-1}	$k_{Cal2init}$ 0.97 s^{-1}	δ_{K12} 0.2
k_{K21} 300 s^{-1}	δ_{K23} 0.001	δ_{K45} 0.2
k_{K32} 5000 s^{-1}	k_{K54} 1500 s^{-1}	
$K_{dK12init}$ 6×10^{-6} M	$K_{dK23init}$ 45×10^{-6} M	$K_{dK45init}$ 20×10^{-6} M
V_{Ka} 33×10^{-3} V	k_{K34} 1000 s^{-1}	k_{K430} 450 s^{-1}

Model's differential equations

Currents charging/discharging hair cell capacitance:

$$-C_m V'_m[t] = g_{Ca}\, m[t]^3\, (V_m[t] - e_{Ca}) + g_K\, (p_{K4}[t] + p_{K5}[t])(V_m[t] - e_K) + (g_{HB} + dg_{HB} \sin[2\,\pi\, f\, t])(V_m[t] - e_{HB})$$

Calcium channel activation:

$$m'[t] = (k_{Ca12init} \exp[(V_m[t] + V_{Ca0})/V_{Cab}] + K_{Cab})(1 - m[t]) - (k_{Ca21init} \exp[-(V_m[t] + V_{Ca0})/V_{Caa}] + K_{Caa})m[t]$$

Calcium concentration:

$$Ca'[t] = -Ug_{Ca}m[t]^3 \frac{V_m[t] - e_{ca}}{2\ \text{faraday vol xi)}} - K_s Ca[t]$$

Gating of the potassium channels:

$$p'_{K1}[t] = clk(-k_1[t]\ Ca[t]\ p_{K1}[t] + k_{K21}\, p_{K2}[t])$$

$$p'_{K2}[t] = clk(k_1[t]\ Ca[t]\ p_{K1}[t] - (k_{K21} + k_2[t]\ Ca[t])\, p_{K2}[t] + k_{K32}\, p_{K3}[t])$$

$$p'_{K3}[t] = clk(k_2[t]\ Ca[t]\ p_{K2}[t] - (k_{K32} + k_{K34})\, p_{K3}[t] + k_{K430} \exp[-V_m[t]/V_{Ka}]\, p_{K4}[t])$$

$$p'_{K5}[t] = clk(k_3[t]\ Ca[t]\ p_{K4}[t] - k_{K54}\, p_{K5}[t])$$

Auxiliary equations:

$$p_{K4}[t] = 1 - p_{K1}[t] - p_{K2}[t] - p_{K3}[t] - p_{K5}[t]$$

$$k_1[t] = k_{K21} \exp[-\delta_{K12}\, V_m[t]/VT]/K_{dK12init}$$

$$k_2[t] = k_{K32} \exp[-\delta_{K23}\, V_m[t]/VT]/K_{dK23init}$$

$$k_3[t] = k_{K54} \exp[-\delta_{K45}\, V_m[t]/VT]/K_{dK45init}$$

To prove that this model can be poised at a Hopf bifurcation, linearize all exponential functions of voltage around the operating point $V_{opPT} = -0.0527$ V, established by first running the oscillator. Then, from the fixed points of this linearization, select the relevant one:

$$p_{K3} = 0.1787, \quad p_{K5} = 0.0950, \quad p_{K1} = 0.1305,$$

$$p_{K2} = 0.5152, \quad p_{K4} = 0.0804, \quad Ca = 0.00001559,$$

$$V_m = -0.05267, \quad m = 0.2324$$

Write down the eigenmatrix describing the behavior of trajectories near this fixed point. It has 28 non-zero entries, of which here we show only the first row consisting of 5 entries:

$$dV'_m/dV_m = -g_{Ca}/C_m\ m^3 - g_K/C_m(p_{K4} + p_{K5}) - g_{HB}/C_m$$

$$dV'_m/dm = -g_{Ca}/C_m(V_m - e_{Ca})\ 3\ m^2$$

$$dV'_m/dp_{K1} = g_K/C_m(V_m - e_K)$$

$$dV'_m/dp_{K2} = g_K/C_m(V_m - e_K)$$

$$dV'_m/dp_{K3} = g_K/C_m(V_m - e_K)$$

Finally, find the eigenvalues and eigenvectors for this eigenmatrix at the fixed point. The eigenvalues having the least negative real part control the dynamical behavior of the oscillator:

$$\lambda = -1.36 + 701.07\, I \qquad \lambda^* = -1.36 - 701.07\, I$$

Increasing g_{HB} above 1.4 nS causes the eigenvalues λ and λ^* to cross the real axis, the definition of a Hopf bifurcation.

We thank Yong Choe and Drs. Pascal Martin, Amit Mehta, Richard Kollmar, Stefan Heller, and Guillermo Cecchi for helpful discussions, and Brian Fabella for computer programming. Members of our research group provided critical comments on the manuscript.

This work was supported by National Institutes of Health Grant DC00241 to Dr. A. J. Hudspeth. During the conduct of this research M.O. was an Associate of Howard Hughes Medical Institute.

REFERENCES

Camalet, S., T. Duke, F. Julicher, and J. Prost. 2000. Auditory sensitivity provided by self-tuned critical oscillations of hair cells. *PNAS.* 97: 3183–3188.

Corey, D. P., and A. J. Hudspeth. 1979. Ionic basis of the receptor potential in a vertebrate hair cell. *Nature.* 281:675–677.

Crawford, A. C., and R. Fettiplace. 1980. The frequency selectivity of auditory nerve fibres and hair cells in the cochlea of the turtle. *J. Physiol.* 306:79–125.

Crawford, A. C., and R. Fettiplace. 1981a. An electrical tuning mechanism in turtle cochlear hair cells. *J. Physiol.* 312:377–412.

Crawford, A. C., and R. Fettiplace. 1981b. Non-linearities in the responses of turtle hair cells. *J. Physiol.* 315:317–338.

Eatock, R. A., D. P. Corey, and A. J. Hudspeth. 1987. Adaptation of mechanoelectrical transduction in hair cells of the bullfrog's sacculus. *J. Neurosci.* 7:2821–2836.

Eguíluz, V. M., M. Ospeck, Y. Choe, A. J. Hudspeth, and M. O. Magnasco. 2000. Essential nonlinearities in hearing. *Phys. Rev. Lett.* 84: 5232–5235.

FitzHugh, R. 1962. Mathematical models of excitation and propagation in nerve. *In* Biological Engineering. H. P. Schwann, editor. McGraw-Hill, 1–85.

Gardner, F. M. 1979. Phaselock Techniques, 2nd Ed. John Wiley and Sons, New York.

Glass, L., and M. C. Mackey. 1988. From Clocks to Chaos: The Rhythms of Life. Princeton University Press.

Herman, H. T., and L. Stark. 1963. Photoreceptor unit transfer characteristics. *J. Neurophysiol.* 26:215.

Holt, J. R., and R. A. Eatock. 1995. Inwardly rectifying currents of saccular hair cells of the leopard frog. *J. Neurophysiol.* 73:1484–1501.

Hudspeth, A. J., and D. P. Corey. 1978. Controlled bending of high-resistance glass microelectrodes. *Am J. Physiol. Cell Physiol.* 234: C56–C57.

Hudspeth, A. J., and R. S. Lewis. 1988a. Kinetic analysis of voltage- and ion-dependent conductances in saccular hair cells of the bullfrog, *Rana catesbeiana. J. Physiol.* 400:237–274.

Hudspeth, A. J. and R. S. Lewis. 1988b. A model for electrical resonance and frequency tuning in saccular hair cells of the bull-frog, *Rana catesbeiana. J. Physiol.* 400:275–297.

Jorgensen, F., and H. Ohmori. 1988. Amiloride blocks the mechano-electrical transduction channel of hair cells of the chick. *J. Physiol.* 403:577–588.

Kros, C. J., J. P. Ruppersberg, and A. Rusch. 1998. Expression of a potassium current in inner hair cells during development of hearing in mice. *Nature.* 394:281–284.

Lewis, R. S., and A. J. Hudspeth. 1983. Voltage- and ion-dependent conductances in solitary vertebrate hair cells. *Nature.* 304:538–541.

Martin, P., and A. J. Hudspeth. 1999. Active hair-bundle movements can amplify a hair cell's response to oscillatory mechanical stimuli. *PNAS* 96:14306–14311.

Meyer, J. J., and H. H. Zakon. 1982. Androgens alter the tuning of electroceptors. *Science.* 217:635–637.

Milhorn, H. T. 1966. The Application of Control Theory to Physiological Systems. W. B. Saunders Co., Philadelphia.

Neiman, A., P. I. Saparin, and L. Stone. 1997. Coherence resonance at noisy precursors of bifurcations in nonlinear dynamical systems. *Phys. Rev. E.* 56:270–273.

Neiman, A., X. Pei, D. Russell, W. Wojtenek, L. Wilkens, F. Moss, H. A. Braun, M. T. Huber, and K. Voigt. 1999. Synchronization of the noisy electrosensitive cells in the paddlefish. *Phys. Rev. Lett.* 82:660–663.

Rieke, F., D. A. Bodnar, and W. Bialek. 1995. Naturalistic stimuli increase the rate and efficiency of information transmission by primary auditory afferents. *Proc. R. Soc. Lond. B.* 262:259–265.

Rieke, F., D. Warland, R. van Stevenick, and W. Bialek. 1997. Spikes: Exploring the Neural Code. MIT Press, Cambridge, MA.

Rosenblatt, K. P., Z-P. Sun, S. Heller, and A. J. Hudspeth. 1997. Distribution of Ca^{2+}-activated K^{+} channel isoforms along the tonotopic gradient of the chicken's cochlea. *Neuron.* 19:1061–1075.

Smotherman, M. S., and P. M. Narins. 1999. The electrical properties of auditory hair cells in the frog amphibian papilla. *J. Neurosci.* 19: 5275–5292.

Strogatz, S. H. 1994. Nonlinear Dynamics and Chaos. Addison-Wesley, Reading, MA.